Electromagnetically-induced-transparency-based paired photon generation

Pavel Kolchin*
Edward L. Ginzton Laboratory, Stanford University, Stanford, California 94305, USA
(Received 4 August 2006; published 26 March 2007)

We describe the theory of paired photon generation in a double-Λ atomic system. Using the Heisenberg-Langevin formalism we evaluate and analyze the spectral generation rates and intensity correlation function for the output fields. Different regimes of parametric down conversion are analyzed. We discuss the influence of the optical depth and Langevin noise fluctuations on the paired photon generation and predict that at the optical depth of 100 or more the contribution of Langevin noise fluctuations is small and therefore Stokes and anti-Stokes photons are generated mostly in pairs. Comparison between the theory and experiments shows good agreement.

DOI: 10.1103/PhysRevA.75.033814 PACS number(s): 42.50.Gy, 32.80.−t, 42.50.Dv, 42.65.Lm

I. INTRODUCTION

Correlated and entangled photon pairs are widely used in quantum communication, quantum cryptography [1], and quantum imaging [2,3]. These photon pairs are usually produced via spontaneous parametric down conversion in nonlinear crystals. A few years ago a different approach to the generation of paired photons had been experimentally demonstrated by two groups, both using electromagnetically induced transparency (EIT) to generate paired photons in an otherwise opaque atomic medium. Working with hot atoms, Lukin and colleagues have demonstrated a correlation between generated pulses of light, as well as storage and delayed extraction [4]. Working with a MOT, Kimble and colleagues have shown the generation of nonclassical photon pairs with a programmable delay [5]. Recently, the Harris research group at Stanford has demonstrated generation and rudimentary wave form control of narrow-band biphotons [6]. More recently, Kolchin and colleagues have shown paired photon generation with a single pump beam in a right-angle geometry [7]. A long coherence length and a controllable bandwidth of the generated paired photons are the advantages of the new approach, which might be useful for such applications as long-distance quantum communication [8] as well as biphoton wave form control and shaping.

This paper describes the theory of correlated paired photon generation in a collection of double-Λ-type atoms. Using the Heisenberg-Langevin method we evaluate and analyze spectral characteristics of the generated Stokes and anti-Stokes photons and their time-correlation properties. The theoretical aspects of paired photon generation in the ground-state approximation have been outlined earlier by Balić *et al.* [6] Here we extend the theoretical treatment to go beyond the ground-state approximation and to investigate the influence of Langevin noise fluctuations on the atomic system.

The schematic of the process considered here is shown in Fig. 1. In the presence of two cw beams termed as the pump and coupling lasers with frequencies ω_p and ω_c, paired spontaneous photons termed as Stokes and anti-Stokes are generated in the atomic cloud and propagate in opposite directions along the z axis. In order to keep the parametric gain small we choose the pump beam to be weak and detuned from the resonance transition $|1\rangle \rightarrow |4\rangle$. The intense coupling beam is tuned to resonance with the $|2\rangle \rightarrow |3\rangle$ transition to enhance the atom-field interaction and provide EIT for the generated anti-Stokes photon. Under such conditions we expect a small fraction of the atomic population to be in the excited states while most of it remains in the ground state $|1\rangle$. The frequencies of the generated photons obey the energy conservation $\omega_s + \omega_{as} = \omega_p + \omega_c$. In the presence of EIT the anti-Stokes photon escapes out of the atomic cloud with very slow group velocity.

We note the connection to earlier work: Two-photon entanglement in type-II SPDC has been analyzed [9]. The possibility of quantum correlated and squeezed fields in the backward-wave EIT system has been predicted [10] and large parametric gain and oscillations have been observed [11]. Control of single photons has been discussed [12]. We also note the early studies on double-Λ atomic systems [13].

Balić and colleagues have shown that at low parametric gain the atomic system can operate in two different regimes [6]. In the first regime, where the group delay is small, the intensity correlation function shows Rabi oscillations. In the second regime, where the optical depth of the atomic sample and the group delay are large, phase matching becomes the dominant process that controls the shape of the intensity correlation function.

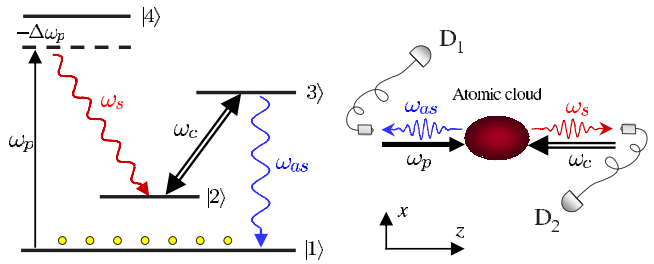

FIG. 1. (Color online). Energy-level diagram and schematic for spontaneous backward-wave paired photon generation in an atomic cloud formed by double-Λ-type atoms. In the presence of the pump and coupling lasers phase-matched, counterpropagating Stokes and anti-Stokes photons are generated into opposite directions.

*Electronic address: pkolchin@stanford.edu

In this paper we review and discuss in detail the system dynamics putting emphasis on the influence of the EIT window on paired photon generation bandwidth. In particular, we reexamine the conditions required for the system to operate in the oscillatory and group delay regimes and discuss corresponding Stokes and anti-Stokes spectral generation rates.

Next, we give the detailed theoretical treatment of paired photon generation without the approximation that the atomic population remains in the ground state. This allows us to properly include and analyze the effect of Langevin noise fluctuation on the atomic system and solve the problem of its return to the ground state after the emission of Stokes and anti-Stokes photon pairs. We also address the important questions: (1) "What are the effects of the optical thickness of the atomic sample on paired and single photon generation?" (2) "Does every Stokes photon have its paired anti-Stokes photon?"

We introduce and derive the biphoton wave function taking into account Langevin noise terms. We also derive and discuss the relation of the Stokes photon count rate to the classical gain coefficient in the Stokes channel.

The paper is organized as follows. We describe the formulation of the problem using the Heisenberg-Langevin method in Sec. II. In Sec. III we describe the linearization procedure and the solution of the field propagation equations. In Sec. IV we obtain the general expression for the quantities of interest: the spectral generation rates of Stokes and anti-Stokes photons and the Glauber two-photon correlation function of time delay τ between Stokes and anti-Stokes photons. In Sec. V we discuss the ideal model of spontaneous parametric down conversion in a crystal with large group delay in one channel. Section VI is devoted to the discussion of paired photon generation in a double-Λ atomic system. We examine the generation rates and the intensity correlation function with and without the assumption that the atomic population is in the ground state. We summarize in Sec. VII.

II. HEISENBERG-LANGEVIN DESCRIPTION OF PAIRED PHOTON GENERATION

We consider a collection of identical double-Λ-type atoms uniformly distributed within a pencil-shaped volume with cross section S and length L. We assume that the atomic sample is optically thin in the transverse direction, so that there is no radiation trapping effect in this direction. No restrictions are imposed on the optical thickness of the atomic sample in the z direction. We also assume that the pump and the coupling beams counter-propagate undepleted through the atomic medium. Under these assumptions we consider propagation of a single transverse spatial mode of radiation along the z axis. The pump and coupling laser beams are treated as classical quantities and their interaction with the medium is described semiclassically. In order to allow for the spontaneous initiation of the parametric fluorescence process, the generated weak Stokes and anti-Stokes fields are described by quantum-mechanical operators, in slowly varying envelope approximation,

$$\hat{E}_j^{(+)} = \sqrt{\frac{\hbar\omega_j}{2\epsilon_0 V}}\hat{a}_j(z,t)\exp(-i\omega_j t + i\vec{k}_j\cdot\vec{z}), \tag{1}$$

where subscript j denotes either Stokes or anti-Stokes photon, $\omega_s=\omega_4-\omega_2+\Delta\omega_{14}$, $\omega_{as}=\omega_3-\omega_1$, and $V=L\times S$ is the interaction volume.

Adopting the notations of Lukin and Fleischhauer [14,15], in the rotating wave approximation we write the interaction Hamiltonian in continuous form as

$$\hat{V} = -\frac{\hbar N}{L}\int_0^L dz\Big(\Delta\omega_{14}\tilde{\sigma}_{44}(z,t) + g_{31}\hat{a}_{as}(z,t)\tilde{\sigma}_{31}(z,t) + \frac{\Omega_c}{2}\tilde{\sigma}_{32}(z,t) + \frac{\Omega_p}{2}\tilde{\sigma}_{41}(z,t) + g_{42}\hat{a}_s(z,t)\tilde{\sigma}_{42}(z,t) + \text{H.c.}\Big), \tag{2}$$

where $\tilde{\sigma}_{jk}(z,t)$ are the collective slowly varying atomic operators, defined in the Appendix, Sec. I, N is the total number of atoms in the atomic ensemble, $\Delta\omega_{14}$ is the detuning of the pump laser from the $|1\rangle\rightarrow|4\rangle$ transition, $\Omega_c=\frac{2\wp_{23}E_c}{\hbar}$, $\Omega_p=\frac{2\wp_{41}E_p}{\hbar}$ are pump and coupling laser Rabi frequencies with E_p, E_c as the complex amplitudes of the electric fields, $g_s=\frac{\wp_{42}\mathcal{E}_s}{\hbar}$ and $g_{as}=\frac{\wp_{31}\mathcal{E}_{as}}{\hbar}$ are the coupling constants with $\wp_{jk}$ as the dipole moment for the $|j\rangle\rightarrow|k\rangle$ transition and $\mathcal{E}_j=\sqrt{\frac{\hbar\omega_j}{2\epsilon_0 V}}$ as the electric field of a single photon.

The propagation of the Stokes and anti-Stokes fields and their interaction with the atoms are described by the set of Maxwell and Heisenberg-Langevin equations. The Heisenberg-Langevin equations are responsible for the atomic evolution,

$$\frac{\partial}{\partial t}\tilde{\sigma}_{jk} = \frac{i}{\hbar}[\hat{V},\tilde{\sigma}_{jk}] - \gamma_{jk}\tilde{\sigma}_{jk} + r_{jk}^A + \tilde{F}_{jk}, \tag{3}$$

where γ_{jk} are the dephasing rates, r_{jk}^A are the spontaneous emission rates, and $\tilde{F}_{jk}(z,t)$ are the collective atomic δ-correlated Langevin noise operators. The full set of the Heisenberg-Langevin equations is shown explicitly in the Appendix, Sec. II.

The fluctuations of δ-correlated collective Langevin noise operators $\tilde{F}_{jk}(z,t)$ is given by

$$\langle\tilde{F}_{jk}(z,t)\tilde{F}_{j'k'}(z',t')\rangle = \frac{L}{N}\mathcal{D}_{jk,j'k'}(z,t)\delta(t-t')\delta(z-z'), \tag{4}$$

where $\mathcal{D}_{jk,j'k'}$ is a Langevin diffusion coefficient. The derivation of Eq. (4) and relevant diffusion coefficients is shown in the Appendix, Sec. IV.

The evolution of the annihilation a_s and creation $a_{as}^\dagger$ operators for the slowly varying Stokes and anti-Stokes fields is described by the coupled propagation equations,

$$\left(\frac{\partial}{\partial t}+c\frac{\partial}{\partial z}\right)\hat{a}_s(z,t)=ig_sN\tilde{\sigma}_{24}(z,t),$$

$$\left(\frac{\partial}{\partial t}-c\frac{\partial}{\partial z}\right)\hat{a}_{as}^{\dagger}(z,t)=-ig_{as}N\tilde{\sigma}_{31}(z,t). \tag{5}$$

The following analysis of the system involves the calculation of the expected values of quantum-field operators and their combinations. We note that in the Heisenberg picture operators evolve and the system is always in its initial state, which in our case corresponds to no Stokes and anti-Stokes input beams at the left and right boundaries.

III. SOLUTION OF COUPLED EQUATIONS

Due to complexity and nonlinearity it is not possible to obtain an analytic solution for the combined set of the field propagation equations and Heisenberg-Langevin equations. Nevertheless, under the condition that Stokes and anti-Stokes fields are much weaker than the coupling and pump fields, and Stokes and anti-Stokes photon densities are much smaller than the atomic density N/V [14], the Heisenberg-Langevin equations can be linearized with Stokes $\hat{a}_s$ and anti-Stokes $\hat{a}_{as}$ fields as perturbation parameters. The linearization procedure is described in detail in the Appendix, Sec. III.

In order to solve the set of the linearized Heisenberg-Langevin Eq. (A10) and coupled propagation Eq. (5), we first Fourier transform them. Then, extracting the solutions for $\tilde{\sigma}_{24}(\omega),\tilde{\sigma}_{31}(\omega)$ and substituting them into Fourier transformed Eq. (5), we obtain the coupled equations for $\hat{a}_s(z,\omega)$ and $\hat{a}_{as}^{\dagger}(z,-\omega)$ in the form

$$\frac{\partial\hat{a}_s}{\partial z}+g_R\hat{a}_s+\kappa_s\hat{a}_{as}^{\dagger}=\sum_{\alpha_i}\xi_{\alpha_i}^{s}\tilde{f}_{\alpha_i},$$

$$\frac{\partial\hat{a}_{as}^{\dagger}}{\partial z}+\Gamma_{as}\hat{a}_{as}^{\dagger}+\kappa_{as}\hat{a}_s=\sum_{\alpha_i}\xi_{\alpha_i}^{as}\tilde{f}_{\alpha_i}, \tag{6}$$

where $g_R(\omega)$, $\Gamma_{as}(\omega)$ are the Raman gain and EIT profile coefficients, respectively, $\kappa_s(\omega)$ and $\kappa_{as}(\omega)$ are Stokes and anti-Stokes mode coupling coefficients, and $\tilde{f}_{\alpha_i}(z,\omega)=\sqrt{N/c}\tilde{F}_{\alpha_i}(z,\omega)$ are the renormalized Langevin noise operators. The sum is taken over the relevant Langevin noise operators $\{\tilde{f}_{21},\tilde{f}_{24},\tilde{f}_{31},\tilde{f}_{34}\}$.

The general solution of Eq. (6) can be written as

$$\begin{pmatrix}\hat{a}_s(L)\\ \hat{a}_{as}^{\dagger}(L)\end{pmatrix}=e^{-\tilde{M}L}\begin{pmatrix}\hat{a}_s(0)\\ \hat{a}_{as}^{\dagger}(0)\end{pmatrix}+\sum_{\alpha_i}\int_0^L dz\,e^{\tilde{M}(z-L)}\begin{pmatrix}\xi_{\alpha_i}^{s}\\ \xi_{\alpha_i}^{as}\end{pmatrix}\tilde{f}_{\alpha_i}, \tag{7}$$

where $\tilde{M}=\begin{pmatrix}g_R\kappa_s\\ \kappa_{as}\Gamma\end{pmatrix}$.

For the following derivation, let us define the coefficients of matrix $e^{-\tilde{M}L}$

$$\begin{pmatrix}A_1 & B_1\\ C_1 & D_1\end{pmatrix}=e^{-\tilde{M}L}. \tag{8}$$

Due to the linearity of Eq. (7), the unknown variables $a_s^{\dagger}(L)$ and $a_{as}(0)$ of the backward-wave problem can be written as a linear combination of the initial boundary values and the noise terms,

$$\begin{pmatrix}\hat{a}_s(L)\\ \hat{a}_{as}^{\dagger}(0)\end{pmatrix}=\begin{pmatrix}A & B\\ C & D\end{pmatrix}\begin{pmatrix}\hat{a}_s(0)\\ \hat{a}_{as}^{\dagger}(L)\end{pmatrix}+\sum_{\alpha_i}\int_0^L dz\begin{pmatrix}P_{\alpha_i}\\ Q_{\alpha_i}\end{pmatrix}\tilde{f}_{\alpha_i}, \tag{9}$$

where

$$\begin{pmatrix}A & B\\ C & D\end{pmatrix}=\begin{pmatrix}A_1-\frac{B_1C_1}{D_1} & \frac{B_1}{D_1}\\ -\frac{C_1}{D_1} & \frac{1}{D_1}\end{pmatrix}, \tag{10}$$

$$\begin{pmatrix}P_{\alpha_i}\\ Q_{\alpha_i}\end{pmatrix}=\begin{pmatrix}1 & -\frac{B_1}{D_1}\\ 0 & -\frac{1}{D_1}\end{pmatrix}e^{\tilde{M}(z-L)}\begin{pmatrix}\xi_{\alpha_i}^{s}\\ \xi_{\alpha_i}^{as}\end{pmatrix}. \tag{11}$$

The coefficients A, B, C, and D are the functions of ω, whereas P_{α_i}, Q_{α_i} are the functions of ω and z.

IV. CHARACTERISTICS OF GENERATED PHOTONS

A. Stokes and anti-Stokes photon generation rates

We evaluate the output generation rates of Stokes and anti-Stokes photons into a single transverse mode, for example, into a pair of mode-matched optical fibers. The generation rates at the corresponding boundaries z_j are

$$R_j=\frac{c}{L}\langle\hat{a}_j^{\dagger}(z_j,t)\hat{a}_j(z_j,t)\rangle, \tag{12}$$

where subscript j denotes either Stokes or anti-Stokes photon, $z_s=L$ and $z_{as}=0$, respectively.

Of importance are the spectral properties of the generated photons. The power spectrum of the output Stokes and anti-Stokes fields are related to their first-order coherence functions $G_j^{(1)}(\tau)=\langle a_j^{\dagger}(z_j,t)a_j(z_j,t+\tau)\rangle$ as

$$R_j(\omega)=\frac{c}{L}\int_{-\infty}^{+\infty}d\tau\,e^{i\omega\tau}G_j^{(1)}(\tau). \tag{13}$$

We use the solutions for $a_s(L,\omega)$ and $a_{as}^{\dagger}(0,-\omega)$ field operators, given by Eq. (9), the commutation relations for the input field operators $[a_j(z_j,\omega),a_j^{\dagger}(z_j,-\omega')]=L/(2\pi c)\delta(\omega+\omega')$, and Eq. (A16). We apply inverse Fourier transformation $a(t)=\int d\omega\,e^{-i\omega t}a(\omega)$ and $a^{\dagger}(t)=\int d\omega\,e^{-i\omega t}a^{\dagger}(-\omega)$ and obtain the Stokes and anti-Stokes generation rates from Eq. (12) in the form

$$R_s=\int\frac{d\omega}{2\pi}\left(|B|^2+\sum_{\alpha_i,\alpha_j}\int_0^L dz\,P_{\alpha_i}^{*}\mathcal{D}_{\alpha_i^{\dagger},\alpha_j}P_{\alpha_j}\right), \tag{14}$$

$$R_{as}=\int\frac{d\omega}{2\pi}\left(|C|^2+\sum_{\alpha_i,\alpha_j}\int_0^L dz\,Q_{\alpha_i}\mathcal{D}_{\alpha_i,\alpha_j^{\dagger}}Q_{\alpha_j}^{*}\right). \tag{15}$$

The integrands of Eqs. (14) and (15) are Stokes and anti-Stokes spectral generation rates, respectively.

As seen from Eqs. (14) and (15), Stokes and anti-Stokes spectral generation rates consist of parametric counts, characterized by the transfer functions $C(\omega)$ and $B(\omega)$, and of noise counts that originate from Langevin noise fluctuations. If the pump is weak and far detuned, $B(\omega)=-C(\omega)$, and therefore the parametric terms in Stokes and anti-Stokes rates are equal. We also note that the contribution of Langevin noise fluctuations to spectral generation rates cannot be neglected and becomes dominant at low optical depth of the atomic sample.

Using the commutator conservation relation for the Stokes field at the right boundary $z=L$, obtained from Eq. (9), the Stokes spectral generation rate can be expressed as

$$R_s(\omega) = |A|^2 - 1 + \sum_{\alpha_i,\alpha_j} \int_0^L dz\, P_{\alpha_i} \mathcal{D}_{\alpha_i,\alpha_j^\dagger} P^*_{\alpha_j}. \tag{16}$$

When the pump is far detuned from the atomic transition and Stokes photon losses are small, the contribution of Langevin noise fluctuation in Eq. (16) is negligible. Thus, the Stokes spectral generation rate can be written as

$$R_s(\omega) \approx |A|^2 - 1. \tag{17}$$

Equation (17) can be interpreted in terms of the quantum theory of linear amplification [16]: in the absence of the Stokes input beam and losses for the Stokes photon, the Stokes generation rate is just the additive noise caused by the amplification process, which is characterized by the gain coefficient $A(\omega)$.

B. Two-photon intensity correlation function and biphoton wave function

In order to address another important issue—the time correlation properties of the generated photons—we calculate the Glauber two-photon correlation function of time delay τ between Stokes and anti-Stokes photons,

$$G^{(2)}_{s\text{-}as}(\tau) = \langle \hat{a}_s^\dagger(L,t)\hat{a}_{as}^\dagger(0,t+\tau)\hat{a}_{as}(0,t+\tau)\hat{a}_s(L,t)\rangle. \tag{18}$$

Using the Stokes and anti-Stokes operators at the boundaries derived earlier [Eq. (9)] and the commutator relations for the input fields, we obtain the intensity correlation function as

$$\begin{aligned} G^{(2)}_{s\text{-}as}(\tau) = \int\int\int\int & d\omega_1\, d\omega_2\, d\omega_3\, d\omega_4 \\ & \times e^{-i\omega_1 t - i\omega_2(t+\tau) - i\omega_3(t+\tau) - i\omega_4 t} \langle \hat{a}_s^\dagger(L,-\omega_1) \\ & \times \hat{a}_{as}^\dagger(0,-\omega_2)\hat{a}_{as}(0,\omega_3)\hat{a}_s(L,\omega_4)\rangle. \end{aligned} \tag{19}$$

The intensity correlation function contains the fourth-order Langevin noise correlations. According to Gaussian moment theorem [17,18] they can be decomposed preserving the order into the sum of the products of second-order Langevin noise correlations. As a result the intensity correlation function can be simplified to

$$G^{(2)}_{s\text{-}as}(\tau) = G^{(1)}_s(0)G^{(1)}_{as}(0) + |\Phi_{s\text{-}as}(\tau)|^2. \tag{20}$$

The first term in Eq. (20) represents flat uncorrelated background; the second term, expressed through $\Phi_{s\text{-}as}(\tau)$ function, describes the correlation part. $\Phi_{s\text{-}as}(\tau)$ is equal to

$$\begin{aligned} \Phi_{s\text{-}as}(\tau) &= \langle \hat{a}_{as}(0,t+\tau)\hat{a}_s(L,t)\rangle \\ &= \frac{L}{2\pi c}\int d\omega e^{i\omega\tau}\left(BD^* + \sum_{\alpha_i,\alpha_j}\int_0^L dz Q^*_{\alpha_i}\mathcal{D}_{\alpha_i^\dagger,\alpha_j}P_{\alpha_j}\right). \end{aligned} \tag{21}$$

We note that $e^{-i\omega_s t - i\omega_{as}(t+\tau)}\Phi_{s\text{-}as}(\tau)$ represents a two-photon wave function or a biphoton on the condition that the peak value of normalized $g^{(2)}_{s\text{-}as} \gg 1$, where $g^{(2)}_{s\text{-}as}(\tau) = G^{(2)}_{s\text{-}as}(\tau)/[G^{(1)}_s(0)G^{(1)}_{as}(0)]$.

Similarly, we can define $\Phi_{as\text{-}s}(\tau) = \langle \hat{a}_s(L,t)\hat{a}_{as}(0,t+\tau)\rangle$. This function can be obtained in the form

$$\Phi_{as\text{-}s}(\tau) = \frac{L}{2\pi c}\int d\omega e^{i\omega\tau}\left(AC^* + \sum_{\alpha_i,\alpha_j}\int_0^L dz P_{\alpha_i}\mathcal{D}_{\alpha_i,\alpha_j^\dagger}Q^*_{\alpha_j}\right). \tag{22}$$

For a wide range of input parameters we numerically verify that $\Phi_{as\text{-}s}(\tau) = \Phi_{s\text{-}as}(\tau)$.

For the case where $\Omega_p/\Delta\omega_{14} \ll 1$ and $\Delta\omega_{14}/\gamma_{14} \gg 1$, we numerically verify that the contribution of Langevin noise fluctuations to $\Phi_{as\text{-}s}(\tau)$ is negligible, therefore Eq. (22) can be simplified to

$$\Phi_{as\text{-}s}(\tau) = \frac{L}{2\pi c}\int d\omega e^{i\omega\tau} AC^*. \tag{23}$$

V. IDEAL SPONTANEOUS PARAMETRIC DOWN CONVERTER

Before we proceed to the discussion of the interesting cases of the atomic correlation functions and photon spectral densities, we want to make an analogy to the well-known parametric down converter in crystals [9]. We consider the ideal model—nondegenerate parametric down converter in which a generated signal photon has a very slow group velocity V_g as compared to an idler photon. We assume that both idler and signal photon escape SPDC without losses, therefore the Langevin noise terms in Eq. (6) can be neglected. In crystals the coupling coefficient can be approximated as a constant over the broad spectral range $\kappa_s(\omega) = \kappa_{as}(\omega) = \kappa$. We also neglect Raman gain $g_R(\omega)$ and approximate EIT profile as $\Gamma(\omega) = -i\omega/V_g$. Under these assumptions the signal and idler photons have identical spectral characteristics and rates. Using Eq. (14), we obtain the photon spectral density $R(\omega)$ and spectrally integrated generation rate $R = 1/(2\pi)\int d\omega R(\omega)$ in the form

$$R(\omega) = |\kappa|^2 L^2\, \mathrm{sinc}^2\left(\frac{\omega L}{2V_g}\right),$$

$$R = V_g|\kappa|^2 L. \tag{24}$$

As seen from Eq. (24), the spectral bandwidth of the SPDC in crystals is limited by $\Delta\omega \sim 2\pi V_g/L$ due to the

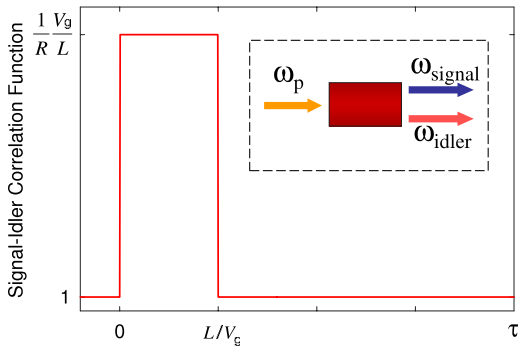

FIG. 2. (Color online) Normalized signal-idler intensity correlation function for the ideal SPDC with the condition of a large group delay L/V_g for a signal photon. R is the paired photon generation rate. (The figure is taken from Ref. [6].)

phase mismatch of the off-centered counts resulting from the group delay in the signal channel. In principle, the bandwidth can be made very small by making the group delay $\tau_g = L/V_g$ large. For the atomic system κ is proportional to the atomic density $\mathcal{N}=N/V$, therefore the spectral density of the generated photons scales as $(\mathcal{N}L)^2$. Taking into account that the EIT-induced group velocity of a wave is $V_g = \Omega_c^2/(2\gamma_{13}\mathcal{N}\sigma_{13})$, where $\sigma_{13}=\wp_{13}^2\omega_{13}/(c\epsilon_0\hbar\gamma_{13})$ is the atomic cross section of the $|1\rangle \rightarrow |3\rangle$ transition, the total count rate scales linearly with $\mathcal{N}L$.

Figure 2 shows the normalized signal-idler intensity correlation function. Since the probability of emitting a photon pair is uniformly distributed along the crystal of length L and the signal photon has a group delay relative to the idler, the $g_{s\text{-}i}^{(2)}(\tau)$ is expected to be the shifted rectangle with the width equal to the group delay $\tau_g=L/V_g$. By varying the group delay we can control the width of the wave form. The peak height of $g_{s\text{-}i}^{(2)}$ is equal to $1/(\kappa L)^2$ and can be interpreted as a duty ratio: $g_{s\text{-}i}^{(2)}=1/(R\tau_g)$. In the regime of very small parametric gain $\kappa L \ll 1$, which can be achieved, for example, by lowering the intensity of the pump, the atomic system can produce highly correlated photon pairs $g_{s\text{-}i}^{(2)} \gg 1$.

VI. EIT-BASED PAIRED PHOTON GENERATOR

Now we turn from the discussion of the ideal SPDC to the discussion of the EIT-based paired photon generator. In the EIT-based generator, coupling between Stokes and anti-Stokes modes is bandwidth limited. Moreover, the generated Stokes photon undergoes Raman gain $g_R(\omega)$, whereas a paired anti-Stokes photon propagates slowly and undergoes absorbtion at the poles of EIT profile $\omega=\pm\Omega_c/2$.

We first obtain the coefficients of Eq. (6) with the assumption that the pump is weak and far detuned from the $|1\rangle \rightarrow |4\rangle$ transition and $\Delta k=(\vec{k}_p+\vec{k}_c-\vec{k}_s-\vec{k}_{as})\hat{z}=0$,

$$\Gamma_{as} = \frac{2i\mathcal{N}\sigma\gamma_{13}(\omega+i\gamma_{12})}{G(\omega)}, \tag{25a}$$

$$g_R = \left(\frac{\Omega_p^2}{2\Delta\omega_{14}^2}\right)\frac{i\mathcal{N}\sigma\gamma_{13}(\omega+i\gamma_{13})}{G(\omega)}, \tag{25b}$$

$$\kappa_s = \kappa_{as} = -\left(\frac{\Omega_p}{2\Delta\omega_{14}}\right)\frac{i\mathcal{N}\sigma\gamma_{13}\Omega_c}{G(\omega)}, \tag{25c}$$

$$\xi_{21}^s = -\left(\frac{\Omega_p}{\Delta\omega_{14}}\right)\frac{\sqrt{2}(\omega+i\gamma_{13})\sqrt{\mathcal{N}\sigma\gamma_{13}}}{G(\omega)}, \tag{25d}$$

$$\xi_{24}^s = -\frac{\sqrt{\mathcal{N}\sigma\gamma_{13}}}{\sqrt{2}\Delta\omega_{14}}, \tag{25e}$$

$$\xi_{31}^s = -\left(\frac{\Omega_p}{\Delta\omega_{14}}\right)\frac{\Omega_c\sqrt{\mathcal{N}\sigma\gamma_{13}}}{\sqrt{2}G(\omega)}, \tag{25f}$$

$$\xi_{34}^s = -\frac{\Omega_c\sqrt{\mathcal{N}\sigma\gamma_{13}}}{2\sqrt{2}\Delta\omega_{14}^2}, \tag{25g}$$

$$\xi_{21}^{as} = \frac{\sqrt{2}\Omega_c\sqrt{\mathcal{N}\sigma\gamma_{13}}}{G(\omega)}, \tag{25h}$$

$$\xi_{24}^{as} = -\left(\frac{\Omega_p}{\Delta\omega_{14}}\right)\frac{\Omega_c\sqrt{\mathcal{N}\sigma\gamma_{13}}}{\sqrt{2}G(\omega)}, \tag{25i}$$

$$\xi_{31}^{as} = \frac{2\sqrt{2}(\omega+i\gamma_{12})\sqrt{\mathcal{N}\sigma\gamma_{13}}}{G(\omega)}, \tag{25j}$$

$$\xi_{34}^{as} = -\left(\frac{\Omega_p}{\Delta\omega_{14}}\right)\frac{\sqrt{2}(\omega+i\gamma_{12})\sqrt{\mathcal{N}\sigma\gamma_{13}}}{G(\omega)}, \tag{25k}$$

where $\mathcal{N}$ is an atom density, $G(\omega)=|\Omega_c|^2-4(\omega+i\gamma_{12})(\omega+i\gamma_{13})$, σ is the absorption cross section for all allowed transitions: $\sigma=\sigma_{14}=\sigma_{24}=\sigma_{23}=\sigma_{13}$.

A. Ground-state approximation

The approximation that the atomic population remains in the ground state $\tilde{\sigma}_{11}=1$ gives two significant diffusion coefficients $\mathcal{D}_{12,21}=2\gamma_{12}$ and $\mathcal{D}_{13,31}=\Gamma_3$ corresponding to F_{21}, F_{31} Langevin noise operators. Due to small atomic population in the excited states, the rest of the diffusion coefficients are approximated as zeros and the corresponding Langevin noise operators are neglected [6].

We numerically examine the emission rates and intensity correlation function for the EIT-based paired photon emitter. We take other parameters similar to those of a Rb MOT: atom density $\mathcal{N}=10^{11}$ atoms per cm^3, atomic cross sections $\sigma=\sigma_{13}=\sigma_{14}=\sigma_{24}=10^{-9}$ cm^2, and dephasing rates equal to one-half of the Einstein A coefficient, i.e., $\gamma_{13}=\gamma_{14}=\gamma_{24}=\gamma_{23}=1.79\times10^7$ radians. We choose the strength and the detuning of the pump laser from the $|1\rangle \rightarrow |4\rangle$ transition as $\Delta\omega_{14}=24\gamma_{13}$ and $\Omega_p/\Delta\omega_{14}=0.1$.

Figure 3 shows the EIT transmission profile and phase mismatch as a function of the detuning of the anti-Stokes frequency ω. We take $\Omega_c=6\gamma_{13}$, $\mathcal{N}\sigma L=11$, and $\gamma_{12}=0$. Figure 4 shows the profiles of the coupling coefficient $|\kappa(\omega)|$ and the Raman gain coefficient $\mathrm{Re}[g_R(\omega)]$ for the same parameters as in Fig. 3.

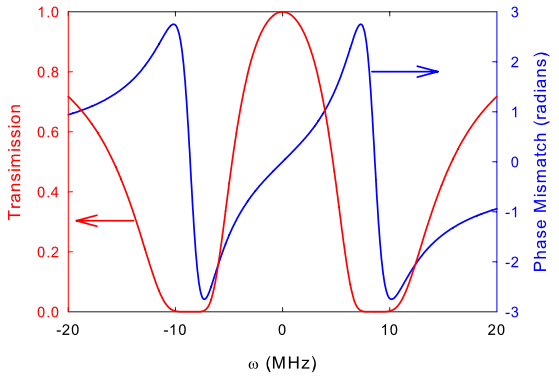

FIG. 3. (Color online) Transmission and phase mismatch as functions of ω.

EIT-based spontaneous emitters allow a variable emission bandwidth. The bandwidth and profile of the spontaneous emission rates are controlled by the strength of the coupling laser Ω_c and the optical depth of the atomic sample $\mathcal{N}\sigma L$. By reducing the strength of the coupling laser, the emission linewidth can be made much smaller than the natural linewidth, with the minimum width ultimately limited by the dephasing rate γ_{12} of the $|1\rangle \rightarrow |2\rangle$ transition. At small optical depth $\mathcal{N}\sigma L < 1$, the Raman gain coefficient $g_R(\omega)$ and the coupling coefficients $\kappa_s(\omega)$, $\kappa_{as}(\omega)$ determine the emission spectrum. At high optical depth $\mathcal{N}\sigma L > 1$, the EIT transmission window and the phase mismatch, introduced by a large group delay in the anti-Stokes channel, affect the spontaneous emission spectrum.

In Figs. 5–7 we show the variations of the coincidence count rate $R_c(\tau)$ in a 1 ns bin and the corresponding Stokes power spectral density depending on the optical depth. With a bin size $\Delta T = 1$ ns much smaller than the correlation time, the coincidence count rate is obtained from the intensity correlation function as $R_c(\tau) = \Delta T (c/L)^2 G^{(2)}_{as\text{-}s}(\tau)$. Compared to the ideal case, described earlier, the intensity correlation function and the emission spectrum for the EIT-based paired photon generator show some interesting features. The shape of the intensity correlation function and the emission profile depend on the relation of three characteristic times. The first is the inverse Rabi frequency of the coupling laser $\tau_r = 2\pi/\sqrt{\Omega_c^2 - \gamma_{13}^2}$, the second is the group delay between Stokes and anti-Stokes photons $\tau_g = L/V_g = 2\gamma_{13}\mathcal{N}\sigma L/\Omega_c^2$,

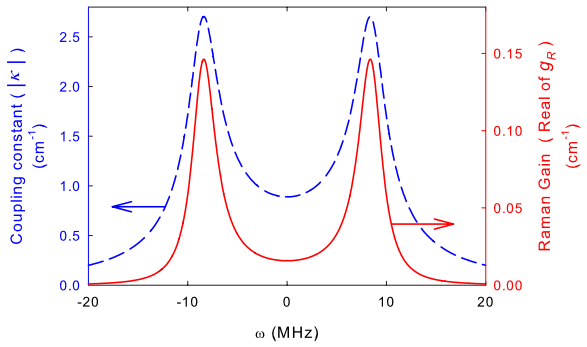

FIG. 4. (Color online) Coupling constant and Raman gain as functions of detuning ω.

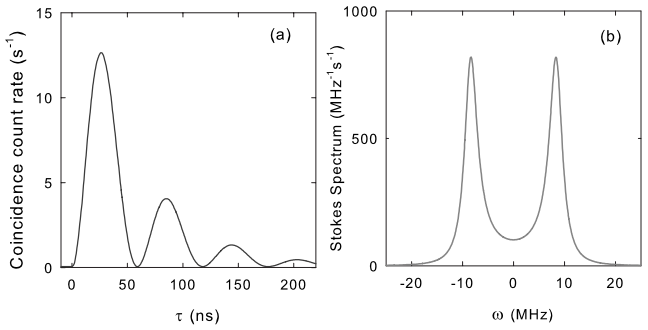

FIG. 5. Oscillatory regime: (a) Coincidence count rate in a 1 ns bin and (b) Stokes spectral generation rate. $\mathcal{N}\sigma L = 0.3$, $\Omega_c = 6\gamma_{13}$, and $\gamma_{12} = 0$.

and the third is a minimal pulse length required to pass through the EIT medium [19] $\tau_{p(min)} = 8\ln(2)\gamma_{13}\sqrt{\mathcal{N}\sigma L}/\Omega_c^2$.

When the EIT effect is small, which occurs, for example, at low optical depth, the atomic system behaves like a single atom [20]. In such a regime the intensity correlation function reveals the damped Rabi oscillations (Fig. 5). The oscillations observed in the intensity correlation function have the time period of $\tau_r = 2\pi/\sqrt{\Omega_c^2 - \gamma_{13}^2}$ and occur on the condition that $\tau_r > \tau_g, \tau_{p(min)}$ and the coupling laser is strong enough to force the oscillations to overcome damping $\Omega_c > \gamma_{13}$. Once the metastable state $|2\rangle$ is excited by the Raman process $|1\rangle \rightarrow |4\rangle \rightarrow |2\rangle$, the probability amplitude between $|2\rangle$ and $|3\rangle$ oscillates due to the strong interaction of the atoms with the resonant coupling beam.

In Fig. 6 we show the intensity correlation function and Stokes emission spectrum in the group delay regime, where $\tau_g > \tau_r$ and $\tau_g > \tau_{p(min)}$. In this regime the width of the intensity correlation function is approximated by τ_g. Moreover, the frequency range over which the spontaneous generation occurs is filtered by the EIT window and mostly controlled by the phase matching in the presence of large group delay in the anti-Stokes channel. A sufficiently wide EIT window $\tau_g > \tau_{p(min)}$ requires high optical depth $\mathcal{N}\sigma L > 10$. In the presence of the nonzero dephasing γ_{12}, the maximum group delay and therefore the maximum width of the correlation function is limited by $\sim 1/\gamma_{12}$.

By increasing the optical depth of the atomic sample, the EIT window can be made substantially larger than the emission bandwidth. A large EIT window might be very useful for such applications as biphoton wave form control and

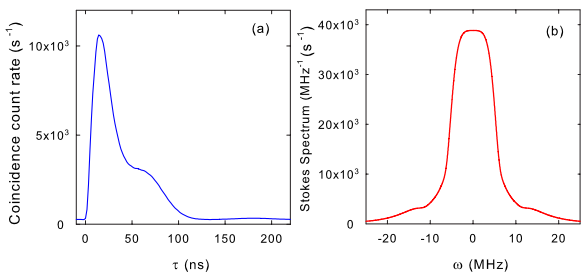

FIG. 6. (Color online) Group delay regime: (a) Coincidence count rate in a 1 ns bin and (b) Stokes spectral generation rate. $\mathcal{N}\sigma L = 20$, $\Omega_c = 6\gamma_{13}$, and $\gamma_{12} = 0$.

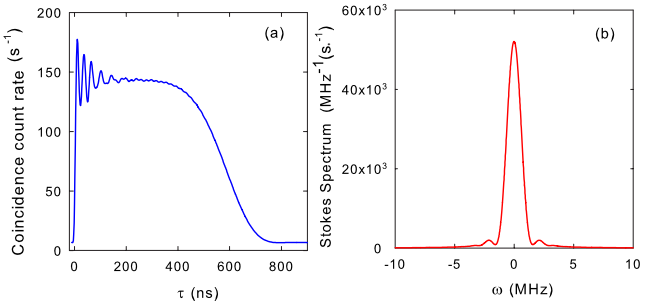

FIG. 7. (Color online) Group delay regime: (a) Coincidence count rate in a 1 ns bin and (b) Stokes spectral generation rate. $\mathcal{N}\sigma L=200$, $\Omega_c=6\gamma_{13}$, $\Omega_p=0.3\gamma_{13}$, and $\gamma_{12}=0$.

shaping [21]. Figure 7 shows the intensity correlation function and the Stokes emission spectrum under such a condition, where $\mathcal{N}\sigma L=200$. The tail of the correlation function decays on the time scale of $\tau_{p(min)}$.

We also note that at high optical depth it becomes possible to achieve the Stokes-anti-Stokes correlation function with the width shorter than the spontaneous decay time $1/(2\gamma_{13})$. Figure 8 shows such a correlation function that is obtained for $N\sigma L=200$ and $\Omega_c=65\gamma_{13}$, where $\tau_r<\tau_g<1/(2\gamma_{13})$.

In Fig. 9 we compare the experimentally observed coincidence count rate with the theoretical prediction of the ground-state approximation. The experimental data (diamonds) is scaled with the duty cycle of 10%. The theoretical curves are scaled by a common factor for each set of the curves. This factor equals the product of the detector efficiencies of 50% each, the filter transmission of 75% each, the fiber-coupling efficiency of 80%, and a theory-experiment discrepancy factor. For Figs. 9(a) and 9(b) the theory-experiment discrepancy factors are equal to 0.10 and 0.14, respectively [6].

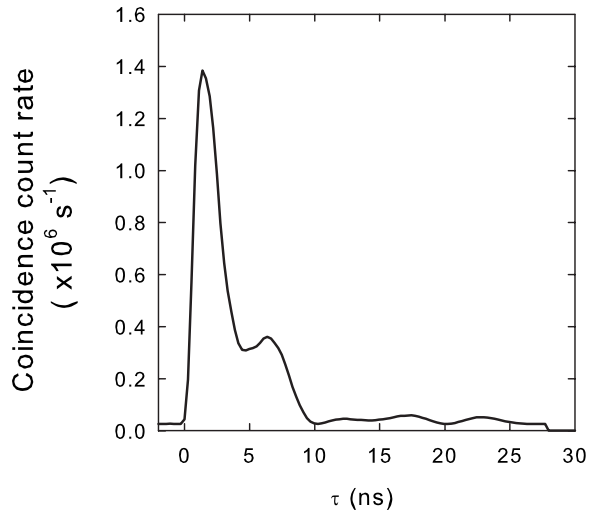

FIG. 8. Intensity correlation function with the correlation time smaller than the spontaneous decay time, $\tau_r<\tau_g<1/(2\gamma_{13})$. $\mathcal{N}\sigma L=200$, $\Omega_c=65\gamma_{13}$, $\gamma_{12}=0$, and $1/(2\gamma_{13})=25$ ns.

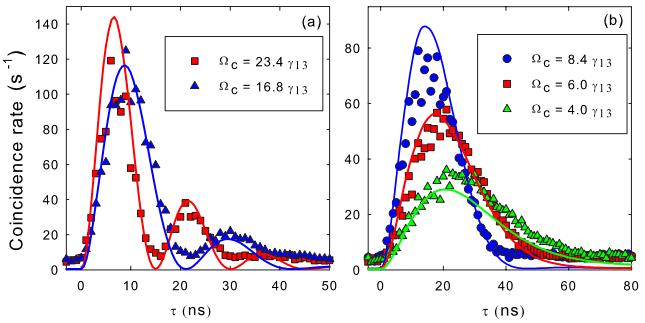

FIG. 9. (Color online) Experimentally measured coincidence count rate in (a) the oscillatory regime and (b) between the oscillatory and group delay regimes. $\mathcal{N}\sigma L=11$, $\Omega_p=0.8\gamma_{13}$, $\Delta\omega_{14}=7.5\gamma_{13}$, and $\gamma_{12}=0.6\gamma_{13}$. The bin size is 1 ns. The experimental data and theory are shown with diamonds and solid lines, respectively. The theoretical curves are scaled vertically by a common factor for each set of the curves. (The figure is taken from Ref. [6].)

B. No ground-state approximation

If the pump is weak and far detuned and therefore most of the atomic population is in the ground state, we verify that the ground-state approximation gives a correct prediction for the biphoton function and the Stokes generation rate. Nevertheless, it does not properly account for an atom's return to the ground state $|1\rangle$. Ideally one would expect the Stokes and anti-Stokes rates to be equal, since an atom, making a complete cycle on the energy-level diagram (Fig. 1), returns to the ground state. Even at zero dephasing rate $\gamma_{12}=0$ of the $|1\rangle\rightarrow|2\rangle$ transition, the ground-state approximation predicts the anti-Stokes generation rate to be smaller than the Stokes generation rate. For example, $R_{as}/R_s=0.65$ for $\mathcal{N}\sigma L=10$, $\Omega_p/\Delta\omega_{14}=0.1$, and $\Omega_c=6\gamma_{13}$.

In order to treat properly an atom's return to the ground state we will retain in Eq. (6) all four Langevin noise operators $\{\tilde{f}_{21},\tilde{f}_{24},\tilde{f}_{31},\tilde{f}_{34}\}$ and take into account a small incoherent population in excited states, resulting from the steady-state solutions of Eqs. (A2a)–(A2f). With these inclusions the solution of Eq. (6) predicts the Stokes and anti-Stokes spectral generation rates to be equal at a zero dephasing rate $\gamma_{12}=0$ [Fig. 10(a)]. A nonzero dephasing rate $\gamma_{12}\neq 0$ reduces EIT and therefore introduces additional losses for anti-Stokes photons. As a result the output Stokes rate exceeds the anti-

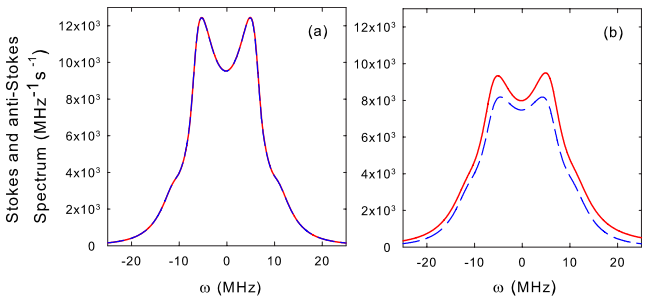

FIG. 10. (Color online) Stokes (solid curve) and anti-Stokes (dashed curve) spectral generation rates at (a) zero dephasing $\gamma_{12}=0$ and (b) nonzero dephasing $\gamma_{12}=0.6\gamma_{13}$. $\mathcal{N}\sigma L=10$, $\Omega_c=6\gamma_{13}\Omega_p=2.4\gamma_{13}$, $\Delta\omega_{14}=24\gamma_{13}$.

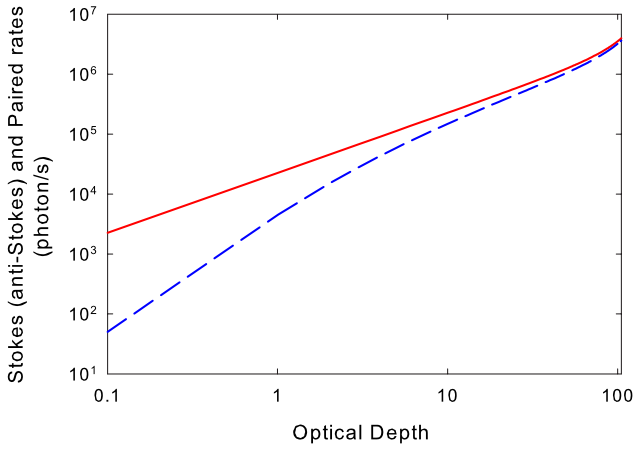

FIG. 11. (Color online) Stokes, anti-Stokes (solid curve), and paired (dashed curve) generation rates as a function of the optical depth. $\Omega_c=5\gamma_{13}$, $\gamma_{12}=0$, $\Delta\omega_{14}=24\gamma_{13}$, and $\Omega_p/\Delta\omega_{14}=0.1$. At an optical depth of 100, the paired rate reaches 90% of the Stokes rate.

Stokes rate. For example, for $\mathcal{N}\sigma L=10$, $\Omega_p/\Delta\omega_{14}=0.1$, $\Omega_c=6\gamma_{13}$, and $\gamma_{12}=0.6\gamma_{13}$ we obtain $R_{as}/R_s\approx 0.8$. The corresponding Stokes and anti-Stokes spectral generation rates are shown in Fig. 10(b). We believe that the "missing" anti-Stokes photons are absorbed and are then reemitted in a solid angle of 4π. The atomic sample is assumed to be optically thin in the radial direction.

Compared to the ideal SPDC, where each generated signal photon has its paired idler photon, the real atomic system has uncorrelated noise counts in both Stokes and anti-Stokes channels that result from Langevin noise fluctuations. In Fig. 11 we examine the dependence of the Stokes (anti-Stokes) and paired count rates on the optical depth $\mathcal{N}\sigma L$. The parameters for the curves are $\gamma_{12}=0$, $\Omega_c=5\gamma_{13}$, $\Delta\omega_{14}=24\gamma_{13}$, and $\Omega_p/\Delta\omega_{14}=0.1$. The paired count rate (R_p) is defined as the area under the Stokes-anti-Stokes coincidence count rate function minus the area under the uncorrelated background. One may show that $R_p\approx 1/(2\pi)\int d\omega|AC^*|^2$. At small optical depth the paired rate scales quadratically with the optical depth and is much smaller than the Stokes rate. At high optical depth the paired rate varies linearly with $\mathcal{N}\sigma L$ and converges logarithmically to the Stokes emission rate.

VII. CONCLUSION

In this paper we study paired photon generation in a double-Λ atomic system. With low parametric gain and high optical depth we show that the system can produce highly correlated photon pairs. The shape of the intensity correlation function and the emission bandwidth depend on the coupling laser Rabi frequency and the optical depth of the atomic sample. Compared to the ideal SPDC, paired photon generation in the double-Λ atomic system is affected by Raman gain in the Stokes channel and EIT in the anti-Stokes channel. EIT, through the absorption at the poles, cuts the emission bandwidth. In order to enter a regime where the EIT window is sufficiently large and therefore the emission bandwidth is controlled to a large extent by the phase-matching process in the presence of large group delay, the optical depth of the atomic sample has to be large $\mathcal{N}\sigma L>10$. High optical depth substantially reduces the influence of Langevin noise fluctuations on paired photon generation so that the Stokes and anti-Stokes photons are generated mostly in pairs. We therefore suggest the use of a cigar-shaped atomic cloud with high optical depth in the longitudinal direction.

ACKNOWLEDGMENTS

The author thanks S. Harris for many helpful discussions and, in particular, for his suggestion of the ground-state approximation. We also thank V. Balić, M. Fleischhauer, M. Lukin, A. André, S. Du, and C. Belthangady for useful discussions. The work was supported by the Defense Advanced Research Projects Agency, the U.S. Air Force Office of Scientific Research, the U.S. Army Research Office, and the Multidisciplinary Research Initiative Program.

APPENDIX

1. Collective slowly varying atomic operators

To describe the quantum properties of the atomic system we use the collective slowly varying atomic operators [15,22–25] $\hat{\sigma}_{jk}(z,t)$, defined as

$$\tilde{\sigma}_{jk}(z,t)=\frac{1}{N_z}\sum_{i\in N_z}|j\rangle_{ii}\langle k|\exp(-i\nu_{jk}t+ik_{jk}z), \tag{A1}$$

where the averaging is done over each atom in a small interval Δz that contains a large number of atoms $N_z\gg 1$. The slowly varying variables are assumed to stay unchanged over Δz. $\nu_{41}=\omega_4-\omega_1+\Delta\omega_{14}$, $\nu_{42}=\omega_4-\omega_2+\Delta\omega_{14}$, $\nu_{14}=-\nu_{41}$, $\nu_{24}=-\nu_{42}$, the rest of $\nu_{jk}=\omega_j-\omega_k$. $k_{31}=\vec{k}_{as}\cdot\hat{z}$, $k_{42}=\vec{k}_s\cdot\hat{z}$, $k_{41}=\vec{k}_p\cdot\hat{z}$, and $k_{32}=\vec{k}_c\cdot\hat{z}$ are the projections of the anti-Stokes, Stokes, pump, and coupling k vectors on the z axis, and $k_{43}=k_{41}-k_{31}$, $k_{21}=-k_{24}+k_{41}$, the rest of $k_{jk}=-k_{kj}$.

2. Heisenberg-Langevin equations

The full set of Heisenberg-Langevin equations for the four-state system consists of 16 equations. Here, we show explicitly ten of them, the other six for the adjoint off-diagonal atomic operators are not shown.

$$\frac{\partial}{\partial t}\tilde{\sigma}_{44}=\tilde{F}_{44}-\Gamma_4\tilde{\sigma}_{44}+i\times\left(\frac{\Omega_p}{2}\tilde{\sigma}_{41}+g_s\hat{a}_s\tilde{\sigma}_{42}-g_s\hat{a}_s^\dagger\tilde{\sigma}_{24}-\frac{\Omega_p^*}{2}\tilde{\sigma}_{14}\right), \tag{A2a}$$

$$\frac{\partial}{\partial t}\tilde{\sigma}_{41}=\tilde{F}_{41}-(\gamma_{41}+i\Delta\omega_{14})\tilde{\sigma}_{41}+i\times\left(-g_{as}\hat{a}_{as}^\dagger\tilde{\sigma}_{43}+g_s\hat{a}_s^\dagger\tilde{\sigma}_{21}+\frac{\Omega_p^*}{2}(\tilde{\sigma}_{11}-\tilde{\sigma}_{44})\right), \tag{A2b}$$

$$\frac{\partial}{\partial t}\tilde{\sigma}_{33} = \tilde{F}_{33} - \Gamma_3\tilde{\sigma}_{33} + i \times\left(g_{as}\hat{a}_{as}\tilde{\sigma}_{31} + \frac{\Omega_c}{2}\tilde{\sigma}_{32} - g_{as}\hat{a}_{as}^{\dagger}\tilde{\sigma}_{13} - \frac{\Omega_c^*}{2}\tilde{\sigma}_{23}\right), \tag{A2c}$$

$$\frac{\partial}{\partial t}\tilde{\sigma}_{32} = \tilde{F}_{32} - \gamma_{32}\tilde{\sigma}_{32} + i \times\left(-g_{as}\hat{a}_{as}^{\dagger}\tilde{\sigma}_{12} + g_s\hat{a}_s^{\dagger}\tilde{\sigma}_{34} + \frac{\Omega_c^*}{2}(\tilde{\sigma}_{33} - \tilde{\sigma}_{22})\right), \tag{A2d}$$

$$\frac{\partial}{\partial t}\tilde{\sigma}_{22} = \tilde{F}_{22} + \Gamma_{32}\tilde{\sigma}_{33} + \Gamma_{42}\tilde{\sigma}_{44} + i \times\left(-\frac{\Omega_c}{2}\tilde{\sigma}_{32} - g_s\hat{a}_s\tilde{\sigma}_{42} + g_s\hat{a}_s^{\dagger}\tilde{\sigma}_{24} + \frac{\Omega_c^*}{2}\tilde{\sigma}_{23}\right), \tag{A2e}$$

$$\frac{\partial}{\partial t}\tilde{\sigma}_{11} = \tilde{F}_{11} + \Gamma_{31}\tilde{\sigma}_{33} + \Gamma_{41}\tilde{\sigma}_{44} + i \times\left(-g_{as}\hat{a}_{as}\tilde{\sigma}_{31} - \frac{\Omega_p}{2}\tilde{\sigma}_{41} + g_{as}\hat{a}_{as}^{\dagger}\tilde{\sigma}_{13} + \frac{\Omega_p^*}{2}\tilde{\sigma}_{14}\right), \tag{A2f}$$

$$\frac{\partial}{\partial t}\tilde{\sigma}_{34} = \tilde{F}_{34} - (\gamma_{34} - i\Delta\omega_{14})\tilde{\sigma}_{34} + i \times\left(\frac{\Omega_p}{2}\tilde{\sigma}_{31} + g_s\hat{a}_s\tilde{\sigma}_{32} - g_{as}\hat{a}_{as}^{\dagger}\tilde{\sigma}_{14} - \frac{\Omega_c^*}{2}\tilde{\sigma}_{24}\right), \tag{A3a}$$

$$\frac{\partial}{\partial t}\tilde{\sigma}_{31} = \tilde{F}_{31} - \gamma_{31}\tilde{\sigma}_{31} + i \times\left(g_{as}\hat{a}_{as}^{\dagger}(\tilde{\sigma}_{33} - \tilde{\sigma}_{11}) - \frac{\Omega_c^*}{2}\tilde{\sigma}_{21} + \frac{\Omega_p^*}{2}\tilde{\sigma}_{34}\right), \tag{A3b}$$

$$\frac{\partial}{\partial t}\tilde{\sigma}_{24} = \tilde{F}_{24} - (\gamma_{24} - i\Delta\omega_{14})\tilde{\sigma}_{24} + i \times\left(\frac{\Omega_p}{2}\tilde{\sigma}_{21} - \frac{\Omega_c}{2}\tilde{\sigma}_{34} + g_s\hat{a}_s(\tilde{\sigma}_{22} - \tilde{\sigma}_{44})\right), \tag{A3c}$$

$$\frac{\partial}{\partial t}\tilde{\sigma}_{21} = \tilde{F}_{21} - \gamma_{21}\tilde{\sigma}_{21} + i \times\left(-\frac{\Omega_c}{2}\tilde{\sigma}_{31} - g_s\hat{a}_s\tilde{\sigma}_{41} + g_{as}\hat{a}_{as}^{\dagger}\tilde{\sigma}_{23} + \frac{\Omega_p^*}{2}\tilde{\sigma}_{24}\right), \tag{A3d}$$

Here, for simplicity, we assume that $\Delta k = (\vec{k}_p + \vec{k}_c - \vec{k}_s - \vec{k}_{as})\hat{z} = 0$. In Eqs. (A2a)–(A2f) and (A3a)–(A3d) Γ_i is the total decay rate from state $|i\rangle$, Γ_{ij} is the decay rate from state $|i\rangle$ to state $|j\rangle$, and γ_{ij} is the dephasing rate between state $|i\rangle$ and state $|j\rangle$. The dephasing rates for the double-Λ system in the absence of the collisional dephasing can be obtained from total decay rates Γ_3 and Γ_4 from state $|3\rangle$ and $|4\rangle$ to two ground states $|1\rangle$ and $|2\rangle$ as

$$\gamma_{31} = \gamma_{32} = \frac{\Gamma_3}{2}, \tag{A4}$$

$$\gamma_{41} = \gamma_{42} = \frac{\Gamma_4}{2}, \tag{A5}$$

$$\gamma_{43} = \frac{\Gamma_3 + \Gamma_4}{2}. \tag{A6}$$

3. Linearization procedure

In zeroth-order perturbation expansion, in which $\hat{a}_s$ and $\hat{a}_{as}$ go to zero, the Heisenberg-Langevin equations for $\tilde{\sigma}_{11}, \tilde{\sigma}_{14}, \tilde{\sigma}_{22}, \tilde{\sigma}_{23}, \tilde{\sigma}_{32}, \tilde{\sigma}_{33}, \tilde{\sigma}_{41}, \tilde{\sigma}_{44}$ atomic operators are decoupled. Under the assumption that pump and coupling beams propagate without depletion, we obtain the steady-state solution for Eqs. (A2a)–(A2f) in form

$$\tilde{\sigma}_{jk}^0 = \langle\tilde{\sigma}_{jk}^0\rangle + \sum \epsilon_{mn}\tilde{F}_{mn}. \tag{A7}$$

With the definition of the denominator as

$$T = \Gamma_{31}(\Gamma_4^2 + 4\Delta\omega_{14}^2 + 2|\Omega_p|^2)|\Omega_c|^2 + \Gamma_{42}(\Gamma_3^2 + 2|\Omega_c|^2)|\Omega_p|^2, \tag{A8}$$

the steady-state expectation values for the zeroth-order atomic operators are equal to

$$\langle\tilde{\sigma}_{11}^0\rangle = \frac{\Gamma_{31}|\Omega_c|^2(\Gamma_4^2 + 4\Delta\omega_{14}^2 + |\Omega_p|^2)}{T}, \tag{A9a}$$

$$\langle\tilde{\sigma}_{22}^0\rangle = \frac{\Gamma_{42}(\Gamma_3^2 + |\Omega_c|^2)|\Omega_p|^2}{T}, \tag{A9b}$$

$$\langle\tilde{\sigma}_{33}^0\rangle = \frac{\Gamma_{42}|\Omega_c\Omega_p|^2}{T}, \tag{A9c}$$

$$\langle\tilde{\sigma}_{44}^0\rangle = \frac{\Gamma_{31}|\Omega_c\Omega_p|^2}{T}, \tag{A9d}$$

$$\langle\tilde{\sigma}_{14}^0\rangle = -\frac{\Gamma_{31}(2\Delta\omega_{14} - i\Gamma_4)|\Omega_c|^2\Omega_p}{T}, \tag{A9e}$$

$$\langle \tilde{\sigma}_{23}^{0} \rangle = \frac{i\Gamma_3\Gamma_{42}\Omega_c|\Omega_p|^2}{T}. \tag{A9f}$$

In the first-order expansion, we substitute the zeroth-order solution for the atomic operators Eq. (A7) into the remaining Heisenberg-Langevin equations for $\tilde{\sigma}_{21},\tilde{\sigma}_{24},\tilde{\sigma}_{31},\tilde{\sigma}_{34}$, and their adjoint. Neglecting higher-order terms like $\epsilon_{mn}\tilde{F}_{mn}\hat{a}_s$ or $\epsilon_{mn}\tilde{F}_{mn}\hat{a}_{as}^{\dagger}$ we obtain the linearized equations. We note that the linearized Eqs. (A3a)–(A3d) for $\tilde{\sigma}_{21},\tilde{\sigma}_{24},\tilde{\sigma}_{31},\tilde{\sigma}_{34}$ represent an independent set of equations and can be decoupled. For clarity we write them in vector form

$$\frac{\partial}{\partial t}\tilde{\boldsymbol{\sigma}}_{\mathbf{1}} = \mathcal{A}\tilde{\boldsymbol{\sigma}}_{\mathbf{1}} + \mathcal{M}\mathbf{a} + \tilde{\mathbf{F}}_{\mathbf{1}}, \tag{A10}$$

where $\tilde{\boldsymbol{\sigma}}_{\mathbf{1}}=\{\tilde{\sigma}_{21},\tilde{\sigma}_{24},\tilde{\sigma}_{31},\tilde{\sigma}_{34}\}$, $\tilde{\mathbf{F}}_{\mathbf{1}}=\{\tilde{F}_{21},\tilde{F}_{24},\tilde{F}_{31},\tilde{F}_{34}\}$, $\hat{\mathbf{a}}=\{\hat{a}_s,\hat{a}_{as}^{\dagger}\}$, matrix $\mathcal{A}$ depends on the dephasing rates γ_{jk}, and pump and coupling laser rabi frequencies Ω_p,Ω_c, matrix $\mathcal{M}$ depends on the zeroth-order solution for the atomic operators $\langle\tilde{\sigma}_{jk}^{0}\rangle$.

4. Langevin noise operators and their diffusion coefficients

By analogy with the collective slowly varying atomic operators $\tilde{\sigma}_{jk}(z,t)$, the collective Langevin noise operators are defined as

$$\tilde{F}_{jk}(z,t) = \frac{1}{N_z}\sum_{z_i\in N_z}\tilde{F}_{jk}^{(i)}(t). \tag{A11}$$

We assume that a Langevin noise operator for a single atom is δ correlated so that

$$\langle \tilde{F}_{jk}^{(i)}(t)\tilde{F}_{j'k'}^{(j)}(t')\rangle = \mathcal{D}_{jk,j'k'}^{(i)}(t)\,\delta(t-t')\,\delta_{ij}, \tag{A12}$$

where $\langle\cdots\rangle$ denotes the average over the reservoir, $\mathcal{D}_{jk,j'k'}^{(i)}(t)$ is the atomic diffusion coefficient for an ith atom.

Now we consider the second-order correlations for the collective Langevin noise operators

$$\langle \tilde{F}_{jk}(t,z)\tilde{F}_{j'k'}(t',z')\rangle = \frac{1}{N_z^2}\sum_{z\,z_i\in N_z}\langle \tilde{F}_{jk}^{(i)}(t)\tilde{F}_{j'k'}^{(i)}(t')\rangle\delta_{zz'}. \tag{A13}$$

Introducing the average atomic diffusion coefficient

$$\mathcal{D}_{jk,j'k'}(t,z) = \frac{1}{N_z}\sum_{z_i\in N_z}\mathcal{D}_{jk,j'k'}^{(i)}(t), \tag{A14}$$

the noise correlations can be expressed as

$$\langle \tilde{F}_{jk}(t,z)\tilde{F}_{j'k'}(t',z')\rangle = \frac{L}{N}\mathcal{D}_{jk,j'k'}(t,z)\,\delta(t-t')\,\delta(z-z'). \tag{A15}$$

In case $\mathcal{D}_{jk,j'k'}(t,z)$ is independent of t, in frequency domain the noise correlations are

$$\langle \tilde{F}_{jk}(\omega,z)\tilde{F}_{j'k'}(\omega',z')\rangle = \frac{L}{2\pi N}\mathcal{D}_{jk,j'k'}\,\delta(\omega+\omega')\,\delta(z-z'). \tag{A16}$$

The diffusion coefficients $\mathcal{D}_{jk,j'k'}$ can be obtained from the Heisenberg-Langevin equations (A2a)–(A2f) and (A3a)–(A3d) using the generalized fluctuation-dissipation theorem [26,27]. Here we show the diffusion coefficients for the Langevin noise operators of interest $\tilde{F}_{21},\tilde{F}_{24},\tilde{F}_{31},\tilde{F}_{34}$ and their adjoint $\tilde{F}_{12},\tilde{F}_{42},\tilde{F}_{13},\tilde{F}_{43}$,

$$\mathcal{D}_{\alpha_i,\alpha_j^{\dagger}} = \begin{pmatrix} 2\langle\tilde{\sigma}_{22}\rangle\gamma_{12}+\langle\tilde{\sigma}_{33}\rangle\Gamma_{32}+\langle\tilde{\sigma}_{44}\rangle\Gamma_{42} & 0 & \langle\tilde{\sigma}_{23}\rangle\gamma_{12} & 0 \\ 0 & \langle\tilde{\sigma}_{22}\rangle\Gamma_4+\langle\tilde{\sigma}_{33}\rangle\Gamma_{32}+\langle\tilde{\sigma}_{44}\rangle\Gamma_{42} & 0 & \langle\tilde{\sigma}_{23}\rangle\Gamma_4 \\ \langle\tilde{\sigma}_{32}\rangle\gamma_{12} & 0 & 0 & 0 \\ 0 & \langle\tilde{\sigma}_{32}\rangle\Gamma_4 & 0 & \langle\tilde{\sigma}_{33}\rangle\Gamma_4 \end{pmatrix}, \tag{A17}$$

$$\mathcal{D}_{\alpha_i^{\dagger},\alpha_j} = \begin{pmatrix} 2\langle\tilde{\sigma}_{11}\rangle\gamma_{12}+\langle\tilde{\sigma}_{33}\rangle\Gamma_{31}+\langle\tilde{\sigma}_{44}\rangle\Gamma_{41} & \langle\tilde{\sigma}_{14}\rangle\gamma_{12} & 0 & 0 \\ \langle\tilde{\sigma}_{41}\rangle\gamma_{12} & 0 & 0 & 0 \\ 0 & 0 & \langle\tilde{\sigma}_{11}\rangle\Gamma_3+\langle\tilde{\sigma}_{33}\rangle\Gamma_{31}+\langle\tilde{\sigma}_{44}\rangle\Gamma_{41} & \langle\tilde{\sigma}_{14}\rangle\Gamma_3 \\ 0 & 0 & \langle\tilde{\sigma}_{41}\rangle\Gamma_3 & \langle\tilde{\sigma}_{44}\rangle\Gamma_3 \end{pmatrix}, \tag{A18}$$

where α_i denotes {21, 24, 31, 34} subspace for the atomic operators, and $\alpha_i^{\dagger}$ denotes {12, 42, 13, 43} subspace for the adjoint atomic operators.

[1] D. Bouwmeester, A. Ekert, and A. Zeilinger, *The Physics of Quantum Information* (Springer-Verlag, Berlin, 2000).
[2] T. B. Pittman, Y. H. Shih, D. V. Strekalov, and A. V. Sergienko, Phys. Rev. A **52**, R3429 (1995).
[3] D. N. Klyshko, Sov. Phys. Usp. **31**, 74 (1988).
[4] C. H. van der Wal, M. D. Eisaman, A. André, R. L. Walsworth,

D. F. Phillips, A. S. Zibrov, and M. D. Lukin, Science **301**, 196 (2003).
[5] A. Kuzmich, W. P. Bowen, A. D. Boozer, A. Boca, C. W. Chou, L.-M. Duan, and H. J. Kimble, Nature **423**, 731 (2003).
[6] V. Balić, D. A. Braje, P. Kolchin, G. Y. Yin, and S. E. Harris, Phys. Rev. Lett. **94**, 183601 (2005).
[7] P. Kolchin, S. Du, C. Belthangady, G. Y. Yin, and S. E. Harris, Phys. Rev. Lett. **97**, 113602 (2006).
[8] L. M. Duan, M. D. Lukin, J. I. Cirac, and P. Zoller, Nature (London) **414**, 6862 (2001).
[9] M. H. Rubin, D. N. Klyshko, Y. H. Shih, and A. V. Sergienko, Phys. Rev. A **50**, 5122 (1994).
[10] M. D. Lukin, A. B. Matsko, M. Fleischhauer, and M. O. Scully, Phys. Rev. Lett. **82**, 1847 (1999).
[11] A. S. Zibrov, M. D. Lukin, and M. O. Scully, Phys. Rev. Lett. **83**, 4049 (1999).
[12] M. D. Lukin and A. Imamoglu, Nature (London) **413**, 273 (2001).
[13] O. Kocharovskaya and P. Mandel, Phys. Rev. A **42**, 523 (1990).
[14] M. Fleischhauer and M. D. Lukin, Phys. Rev. A **65**, 022314 (2002).
[15] M. Fleischhauer and M. D. Lukin, Phys. Rev. Lett. **84**, 5094 (2000).
[16] M. Haus, Phys. Rev. **128**, 2407 (1962).
[17] L. Mandel and E. Wolf, *Optical Coherence and Quantum Optics* (Cambridge University Press, Cambridge England, New York, 1994).
[18] W. H. Louisell, *Quantum Statistical Properties of Radiation* (Wiley, New York, 1973).
[19] S. E. Harris and L. V. Hau, Phys. Rev. Lett. **82**, 4611 (1999).
[20] M. O. Scully and C. H. R. Ooi, J. Opt. B: Quantum Semiclassical Opt. **6**, S816 (2004).
[21] In a right-angle geometry, where Stokes and anti-Stokes photons are generated and collected at right angles from the direction of the pump-coupling axis, applying the absorption mask on the pump beam allows us to create a biphoton with a prescribed wave form.
[22] F. A. Hopf and P. Meystre, Phys. Rev. A **12**, 2534 (1975).
[23] M. Fleischhauer and T. Richter, Phys. Rev. A **51**, 2430 (1995).
[24] L. You, J. Mostowski, and J. Cooper, Phys. Rev. A **46**, 2903 (1992).
[25] D. Polder, M. F. H. Schuurmans, and Q. H. F. Vrehen, Phys. Rev. A **19**, 1192 (1979).
[26] M. Sargent, M. O. Scully, and W. E. Lamb, *Laser Physics* (Addison-Wesley, Reading, MA, 1974).
[27] M. O. Scully and M. S. Zubairy, *Quantum Optics* (Cambridge University Press, Cambridge, New York, 1997).